International Communications in Heat and Mass Transfer 167 (2025) 109269

Contents lists available at ScienceDirect

International Communications in Heat and Mass Transfer

journal homepage: www.elsevier.com/locate/ichmt

A novel methodology for calculating thermal conductivity of natural hollow fibers with validation in nonwoven fabric structures

Seyyed Mohsen Mortazavinejad [a,*], Mostafa Alakhdar [a], Ludwig Vinches [b], Stéphane Hallé [a]

[a] Dept. of Mechanical Engineering, École de Technologie Supérieure, 1100 Notre-Dame West, Montréal, QC H3C 1K3, Canada
[b] Dept. of Environmental and Occupational Health, University of Montreal, 2375 Chemin. de La Côte-Sainte-Catherine, Montréal, QC H3T 1A8, Canada

ARTICLE INFO

Keywords:
Porous media
Fibrous materials
Composite thermal conductivity
Heat transfer
Thermal insulation
Hollow fibers

ABSTRACT

Natural fibers, especially hollow ones, are increasingly used in nonwoven insulation structures for their superior thermal insulation performance, renewability, and biodegradability, as hollow fibers offer lower thermal conductivity than solid fibers. However, accurately measuring the thermal conductivity of single hollow fibers, particularly given their extremely small diameter (10–50 μm) and thin wall thickness (around 1 μm), remains challenging, limiting the understanding of their role in composite materials. To address this, a novel approach combines experimentally measured bulk thermal conductivity with theoretical models for effective and radiative thermal conductivity in a numerical iterative process. Additionally, a theoretical framework was established to analyze composite thermal conductivity and was validated through experimental bench tests. After successfully predicting the thermal conductivity of a single hollow fiber, results indicated minimal anisotropy in the examined fibers that can be attributed to their thin wall thickness. Furthermore, the study demonstrated that fiber arrangement had little impact on thermal conductivity in highly porous structures, while decreasing fiber diameter significantly reduced radiative thermal conductivity due to increased scattering. These findings provide a comprehensive framework for evaluating the thermal behavior of hollow fibers and optimizing natural-fiber-based insulation materials, contributing to the development of more efficient and sustainable thermal insulation solutions.

1. Introduction

Nonwoven fibrous materials have gained significant popularity in industries such as construction and textiles due to their high porosity, affordability, and lightweight nature. Their versatility has led to numerous applications, with thermal insulation being one of the most prominent [1,2]. Thermal insulation fibrous materials produced from mineral and fossil-based sources are currently popular, primarily because of their cost-effectiveness [3]. However, their production processes are energy-intensive and contribute significantly to CO_2 emissions. Additionally, these materials release harmful pollutants, including toxic gases and particulates such as SO_x and NO_x, which exacerbate environmental pollution [4,5]. Their lack of biodegradability further poses challenges, particularly with waste management at the end of their lifecycle [6]. In contrast, plant-based natural fibers have emerged as a sustainable alternative for insulation due to their widespread availability, renewability, recyclability, biodegradability, and ability to store carbon [7–9]. The diameter of natural fibers, a critical parameter influencing their thermal insulation properties [10], typically ranges in the micron scale ($> 10\ \mu m$), while the pore size of these fibrous structures can vary from several microns to several millimeters [11–13]. Bulk thermal conductivity of natural fiber-based insulation materials typically ranges from 0.03 to 0.1 W/m·K [14], depending upon production technology and structural characteristics. Of these aspects, thickness and porosity have been identified as the most critical factors affecting bulk thermal conductivity [15] which is typically measured experimentally using techniques such as the guarded hot plate and heat flow meter [16]. Theoretically, thermal conductivity of the fibrous materials can be modeled using several approaches that account for fiber arrangement and material composition. The series and parallel models provide simplified representations, assuming homogeneous components (air and fiber) are arranged either perpendicular or parallel to the heat flow direction, respectively. More advanced models, such as the Maxwell-Eucken (ME) models (ME 1 and ME 2) describe composites where one phase forms a continuous matrix and the other a dispersed inclusion. Additionally, the effective medium theory offers a framework

* Corresponding author.
E-mail address: seyyed-mohsen.mortazavinejad.1@ens.etsmtl.ca (S.M. Mortazavinejad).

https://doi.org/10.1016/j.icheatmasstransfer.2025.109269

Available online 28 June 2025

for materials with randomly distributed phases, allowing for a more realistic representation of nonwoven fibrous structures [17–20]. The thermal conductivity of fibers is a critical parameter in these theoretical models, as it is essential for accurately predicting the overall thermal performance of nonwoven structures. However, accurately measuring the thermal conductivity of single hollow fibers is particularly challenging, especially given their small diameter (10–50 μm) and thin wall thickness (around 1 μm), which limits the understanding of their role in composite materials [10]. In this regard, Kawabata [21] developed an apparatus to measure the thermal properties of 14 fiber types. For longitudinal thermal conductivity, approximately 10,000 fibers were clamped with a 20 mm width and 3 mm gap, exposed to a 20 mW heat flux. To measure transverse conductivity, a composite film of aligned fibers embedded in epoxy (≈80 % fiber volume fraction) was fabricated, with dimensions of 50 × 50 mm^2 and a thickness of 0.5–1 mm. The results revealed strong anisotropy in some fibers, with ratios of 11.85 for cotton and 12.64 for silk, indicating significant differences between axial and transverse conductivity. While Kawabata's method addressed both directions, the composite film approach was used only for the transverse case, and the reason for not applying it to the axial direction remains unclear. Some other works was explored to measure the thermal conductivity of natural fibers. For instance, Asangwing [22] explored palm fiber thermal conductivity by reinforming lateritic soil, similar to study done by Kawabata through making a composite [21]. Damfeu et al. [23] developed a bench test based on the transient method using asymmetric hot plate to measure the thermal conductivity of natural fibers. While this study made significant advancements, it did not account for the anisotropic nature of hollow fibers. *Al*-Sulaiman et al. [24] proposed correlations derived from finite element analysis to estimate fiber thermal conductivity using the known thermal conductivity of a fiber-reinforced composite laminate (FRCL) and its constituent materials. Their model assumes the FRCL is cured under high pressure, eliminating the presence of air voids. Additionally, a numerical approach was introduced, wherein the thermal conductivity of a fiber was calculated by embedding it in a resin composite, followed by prediction models using series and parallel arrangements. However, this study primarily focused on solid fibers [25].

Understanding and accurately determining the thermal conductivity of such hollow fibers remains a key challenge in advancing the predictive models for nonwoven fibrous materials. In this regard, this study introduces a novel approach specifically designed for hollow fibers. In this paper, a methodology is established by combining theoretical and experimental approaches to calculate the thermal conductivity of hollow fibers. Determining the thermal conductivity of individual hollow fibers is crucial, as it enables designers to strategically mix fibers based on their individual thermal conductivity values, thereby optimizing nonwoven fabric structures for superior thermal insulation performance. To this end, the study focuses on three types of natural fibers: kapok, milkweed (MW), and polylactic acid (PLA). The selection of these three fibers is based on the industrial partner relevance, local availability, and advantageous physical properties. Kapok and MW are well-known for their hollow structures [26,27], while the hollow nature of PLA fibers is less certain and is further investigated during this study. These fibers are selected for their potential to reduce thermal conductivity, even though, to the best of our knowledge, no definitive values for their thermal conductivity have been reported in the literature. Building upon this, the thermal conductivity of a composite composed of these fibers with varying densities is investigated—a novel consideration that has not been addressed in previous studies on effective thermal conductivity of nonwovens. To ensure the accuracy of the results, a bench test was developed to compare experimental measurements of thermal conductivity with our theoretical predictions. Finally, additional parameters such as fiber diameter and fiber orientation, and their roles in optimizing the thermal insulation performance of natural fiber-based composite materials, are also investigated.

2. Materials and methods

2.1. Materials

MW and kapok fibers share lightweight, hollow structures with high porosities of 82 % and 77 %, respectively, contributing to their excellent thermal insulation properties. MW fibers have diameters of 20–50 μm while kapok fibers have diameters of 10–25 μm and wall thicknesses of 0.5–2 μm. Both fibers feature a wax-coated surface, enhancing their hydrophobicity and suitability for insulation applications [26,27]. Also, PLA, a biodegradable thermoplastic derived from renewable sources, offers low thermal conductivity and sustainability, presenting an eco-friendly alternative to fossil-fuel-based insulating materials [28]. Due to variations in fiber suppliers and the associated uncertainties in the literature regarding mean diameter, wall thickness, and wall density, it was essential to measure and examine these features directly in this study.

The mean inner diameter (d_i) and wall thickness (t) of the fibers are measured using scanning electron microscopy (SEM). Gold-coated fiber membranes are analyzed with a Hitachi S3600N SEM. d_i and t are determined from cross-sectional images by measuring 50 fibers using ImageJ software. The wall density (ρ_w) of the fibers is calculated using a gas pycnometer (Anton Paar Ultrapyc 5000), with ten tests conducted for each fiber type. Assuming a circular cross-section, the fiber density (ρ_f) is calculated using eq. (1), where (A_i) and (A_o) represent the inner and outer areas of the fiber's cross-section [29].

$$\rho_f = \left(\frac{A_o - A_i}{A_o}\right)\rho_w \tag{1}$$

The measured geometric properties, including d_i and t, along with ρ_w and ρ_f for the three fibers, are summarized in Table 1:

The SEM analysis revealed that the kapok and MW fibers (Fig. 1(a) and (b)) have a hollow structure, while the PLA fibers (Fig. 1 (c)) lack a hollow structure and can be considered solid, as no measurable wall thickness is observed. Additionally, comparisons with other studies show variations in reported values for diameter, wall thickness, wall density, and consequently fiber density [29–32]. These discrepancies likely arise from differences in fiber suppliers, origins, and processing methods, which can influence the structural and physical properties of the fibers. Therefore, such variations emphasize the importance of direct characterization for accurate property determination.

Although some studies have investigated the thermal properties of kapok, MW, and PLA, to the best of our knowledge, no data on the thermal conductivity of the individual fibers is available in the literature. Some papers reference bulk thermal conductivity values for these materials but lack the specific insights necessary for single-fiber thermal analysis. For example, a study has reported that when the bulk density of fabric structures varies from 5 to 40 kg/m^3, the thermal conductivity of kapok falls within the range of 0.03 to 0.04 W/m·K [32]. Additionally, for MW samples another study indicated that thermal conductivity values between 0.031 and 0.032 W/m·K for densities ranging from 5 to 30 kg/m^3 [26,33]. However, these values fail to provide insight into the thermal conductivity of individual fibers, highlighting the gap in the literature. This gap underscores the necessity of developing a new methodology to calculate the thermal conductivity of individual fibers.

Table 1
Geometric properties, wall density, and calculated fiber density of kapok, MW, and PLA.

Fiber	d_i (μm)	t (μm)	ρ_w (kg/m^3)	ρ_f (kg/m^3)
kapok	24.05 ± 2.62	0.84 ± 0.38	1553.4 ± 24.7	196.9
MW	24.95 ± 3.87	1.03 ± 0.40	1721.0 ± 41.4	252.3
PLA	15.02 ± 2.19	–	1277.0 ± 3.3	1277.0

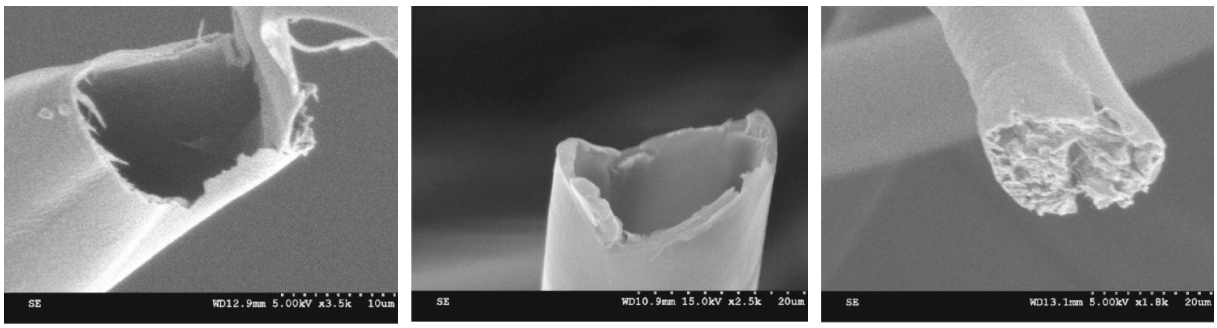

(a) kapok (b) MW (c) PLA

Fig. 1. SEM images of the studied fibers: (a) Kapok, (b) MW, and (c) PLA.

2.2. Methods

Heat transfer in porous materials made from fibers encompasses several mechanisms, as shown in Fig. 2. These include thermal conduction through the solid fiber framework (k_{solid}) and the air within the pores (k_{gas}), convective heat transfer (k_{conv}) caused by gas movement, and radiative heat transfer (k_{rad}) occurring between the fibers [10].

To address the complexities of heat conduction in porous materials composed of fibers and air, the concept of effective thermal conductivity (k_{eff}) is introduced, which represents the combined conductive behavior of the solid and gaseous phases. Consequently, when measuring the thermal conductivity of a sample made of fibers, k_{sample}, it is expected to conform to the mathematical expression given in eq. (2):

$$k_{sample} = k_{eff} + k_{rad} + k_{conv} \tag{2}$$

Before proceeding with the derivation of this formulation, it is important to consider the potential influence of natural convection within fibrous structures. Natural convection in fibrous insulation materials depends on the balance between gravitational forces and viscous resistance, measured by the Rayleigh number (Ra). For natural convection to occur in fibrous materials, Ra must exceed the critical value of ($4\,\pi^2 \approx 39.5$) [34]. In a 1 cm thick fibrous medium made up of fibers with a diameter of 10 μm and a volume fraction of 1 %, the Ra number remains well below 1 even with a 100 K temperature difference [35]. This demonstrates that the conditions required for natural convection are not met in typical fibrous insulation structures, making its effect on heat transfer negligible.

With this simplification, eq. (2) is reduced to eq. (3), forming the basis for the proposed methodology.

$$k_{sample} = k_{eff} + k_{rad} \tag{3}$$

Considering eq. (3), the new methodology leverages the relationship between the sample's thermal conductivity and the effective and radiative thermal conductivity of its constituent fibers. By utilizing this connection, it becomes possible to determine the fiber thermal conductivity for cases where no prior data exists. In the following sections, the treatment of each contributing term is detailed, culminating in the description of the approach used to solve the final equation to calculate the single fiber thermal conductivity.

2.2.1. Sample thermal conductivity - k_{sample}

Similar to previous studies on fiber thermophysical properties, the bulk thermal conductivity of fiber samples can be measured using both steady-state and transient instruments [16]. In this study, the Trident

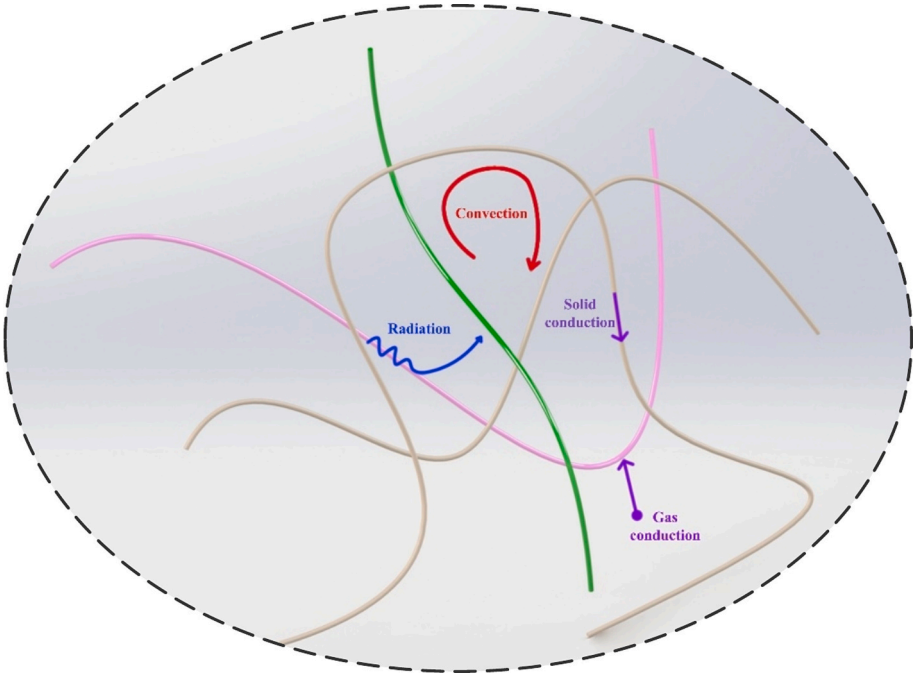

Fig. 2. Heat transfer modes inside fibrous materials.

device (C-Therm Technologies Ltd.), based on the transient plane source method, is used for thermal conductivity measurement. The device works by applying a known current to the sensor's spiral heating element, generating a small amount of heat. A guard ring surrounds the sensor coil to ensure one-dimensional heat transfer into the sample. The heat applied causes a temperature rise (around 2 °C) at the interface between the sensor and the sample, resulting in a voltage change. The rate of voltage increase is used to determine the sample's thermal properties. The rate of voltage increase is used to determine the sample's thermal properties. The measurement uncertainty of the Trident is specified as 5 %, which defines the accuracy of the reported thermal conductivity values. To measure thermal conductivity at varying densities, a compression test accessory is integrated with the sample holder to compress the sample, enabling the adjustment of bulk density. The way the thermal conductivity is measured is illustrated in Fig. 3, showcasing the fiber sample (a), the Trident device (b), the sensor (c), and the integrated compression test accessory (d), with five tests were performed for each of the samples.

2.2.2. *Effective thermal conductivity* - k_{eff}

k_{eff} reflects the combined influence of the thermal conductivities and volume fractions of fibers (k_s, v_s) and air (k_f, v_f). Islam and Bhat examined eq. (4) and eq. (5) to calculate the effective thermal conductivity of their samples. However, the discrepancy between their initial results and the values predicted by these equations highlighted their limitations in accurately capturing porous composite structures. To address this, a new model was developed by them, combining ME 1 and ME 2 for random arrangement of fibers, illustrated in Fig. 4. In ME1, phase 1 (air) is considered the continuous phase while phase 2 (fiber) is dispersed; in ME2, the roles are reversed. This consideration aligns with the experimental results, as shown in eq. (6) [36]:

$$k_{eff,ME\ 1} = k_s \frac{k_s + k_f - (k_s - k_f)v_f}{k_s + k_f + (k_s - k_f)v_f} \tag{4}$$

$$k_{eff,ME\ 2} = k_f \frac{k_f + k_s - (k_f - k_s)v_s}{k_f + k_s + (k_f - k_s)v_s} \tag{5}$$

$$k_{eff} = \frac{k_{eff,ME\ 1} \times k_{eff,ME\ 2}}{(v_f \times k_{eff,ME\ 1}) + (v_s \times k_{eff,ME\ 2})} \tag{6}$$

In eq. (4) to (6), k_s represents the thermal conductivity of a solid fiber. However, since two of the three fibers under study are hollow, k_s must be adjusted to account for the hollow structure to ensure accurate application of the new model. To accurately apply the new model, the analysis specifically targets the fiber structure—distinct from the fabric structure—by treating it as a composite cylinder comprising the fiber material and stationary air. The thermal conductivity of the composite fiber along its axis $(k_{s,a})$ and perpendicular to its axis $(k_{s,t})$ is determined using eq. (7) and (8), where $(h = \left(\frac{d_i}{d_o}\right)^2)$ and d_o is outer diameter of the fiber, $(c_1 = \frac{k_f + k_s}{k_f - k_s})$ and $(c_2 = \frac{k_f - k_s}{k_f + k_s})$ [37,38]:

$$k_{s,a} = k_s + (k_f - k_s)h \tag{7}$$

$$k_{s,t} \approx k_s \left(1 + \frac{2h}{c_1 - h + c_2(0.30584h^4 + 0.013363h^8)}\right) \tag{8}$$

Given that a portion of the fiber aligns parallel to the heat flow direction and another portion aligns perpendicular, an average thermal conductivity $(k_{s,ave})$ can be calculated by equally weighting $k_{s,a}$ and $k_{s,t}$. This average value, expressed by eq. (9), replaces k_s in the analysis expressed by eq. (4) to (6).

$$k_{s,ave} = 0.5k_{s,a} + 0.5k_{s,t} \tag{9}$$

It is important to note that while eq. (4) to (6) were originally derived under the assumption of a random fiber arrangement, incorporating $k_{s,ave}$ in place of k_s in expression (9) required assigning proportional values for fibers oriented parallel and perpendicular to the heat transfer direction. This consideration, along with the assumption of equal weighting, led to the formulation of eq. (9). The accuracy of this assumption is thoroughly examined in Section 3.5.

Furthermore, in eq. (4) to (6), v_f and v_s are based on a composite of solid fiber and air. However, since the fiber itself is a composite with enclosed air, the volume fractions must be adjusted. To account for this, inner (ε_i) and outer (ε_o) porosities are defined, representing the volume fraction of air inside the fibers and between the fibers, respectively. The total porosity (ε), is the sum of these two components. Consequently, v_f and v_s in eq. (4) to (6) must also be modified to reflect this adjustment. To achieve this, ε_i, ε_o, and ε should be calculated using eq. (10) to (12), where ρ_{bulk} represents the bulk density of the fabric structure [39]:

$$\varepsilon = 1 - \frac{\rho_{bulk}}{\rho_w} \tag{10}$$

$$\varepsilon_o = 1 - \frac{\rho_{bulk}}{\rho_f} \tag{11}$$

$$\varepsilon_i = \rho_{bulk}\left(\frac{1}{\rho_f} - \frac{1}{\rho_w}\right) \tag{12}$$

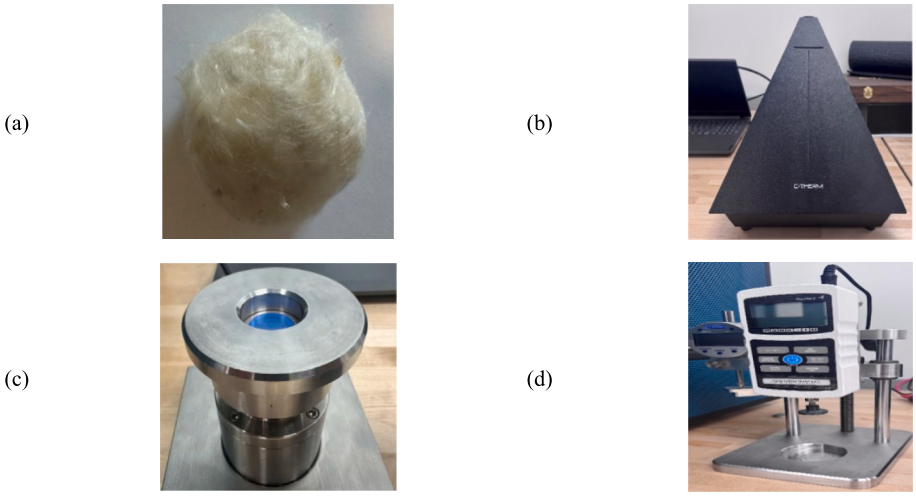

Fig. 3. Schematic representation of the measurement setup: (a) fiber sample, (b) Trident device, (c) sensor, and (d) compression test accessory.

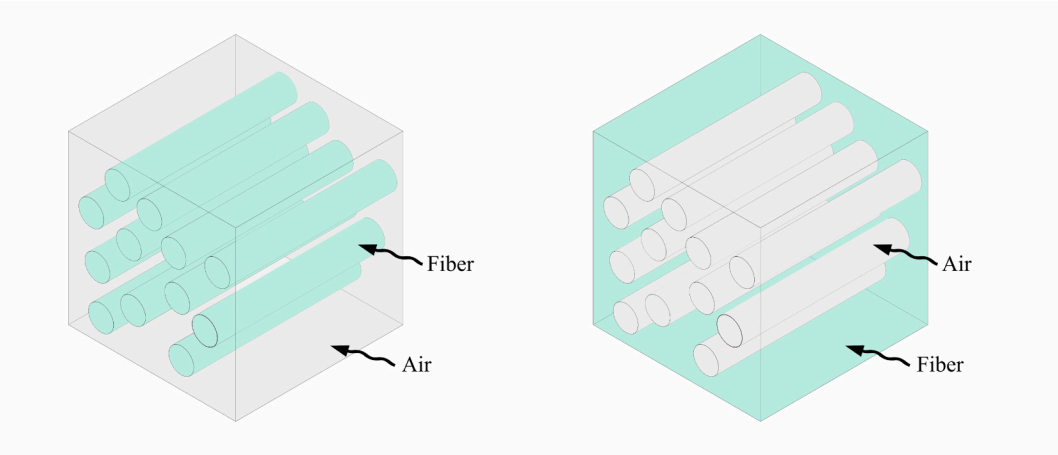

Fig. 4. Schematic representation of ME 1 (a) and ME 2 (b) considering fiber and air components.

After determining the total, inner, and outer porosities, ν_s in eq. (4) to (6) should be replaced by $\nu_s + \varepsilon_i$, and ν_f should be replaced by ε_o to incorporate the effect of the hollowness of the fiber in the calculation of k_{eff}.

2.2.3. *Radiative thermal conductivity* - k_{rad}

Some studies suggest that radiation heat transfer in fibrous insulation materials is negligible at room temperature [36,40]. However, to evaluate this claim, it is important to account for factors such as the properties of the fiber, porosity, pore size, shape, and surface conditions, all of which influence the contribution of radiation. The significance of radiative heat transfer also depends on the optical thickness of the medium. For optically thick regions, the Rosseland diffusion approximation is commonly used, while the Bankvall model is more suitable for optically thin regions [41–43]. For natural fiber-based fabric structures, regions with porosities above 98 % are better characterized as optically thin, while those with lower porosities are optically thick, as demonstrated in [10]. Rosseland mean extinction coefficient, β_r, denotes as eq. (13), quantifies the rate at which radiation intensity decays within a material:

$$\frac{1}{\beta_r} = \int_{\lambda_1=0}^{\lambda_2} \frac{-L}{\ln(\tau)} \frac{2\pi\hbar^2 c^3 \exp\left(\frac{\hbar c}{K_B T}\right)}{4K_B \sigma \lambda^6 T^5 \left(\exp\left(\frac{\hbar c}{K_B T}\right) - 1\right)} d\lambda \tag{13}$$

Where L is the thickness of the fabric structure, τ is the transmittance of the fabric structure, $\hbar$ is the Plank's constant, K_B is the Boltzmann constant, σ is the Stefan Boltzmann constant, and c is the speed of light. It has been well established that more than 80 % of thermal radiation falls within the wavelength range of 2.5 μm (= λ_1) and 25 μm (=λ_2) at temperatures below 973 K, and the spectral transmittance is typically evaluated within this range [44]. Since calculating the Rosseland mean extinction coefficient for optically thick regions can be challenging, an alternative and more practical approach is to use other suggested expressions. For instance, k_{rad} can be approximated by eq. (14) [45]:

$$k_{rad} = \frac{4\sigma {T_0}^3 d_o}{\nu_s \epsilon} \tag{14}$$

Where, T_0 represents the mean temperature of the fabric structure considering T_1 and T_2, and ϵ is the emissivity of the boundary surfaces, shown in Fig. 5.

In this study, direct measurement of the spectral transmittance of the fabric structure was not performed. Instead, using eq. (14), which assumes that radiation occurs primarily between nearly opaque fibers—makes explicit calculation of transmittance unnecessary.

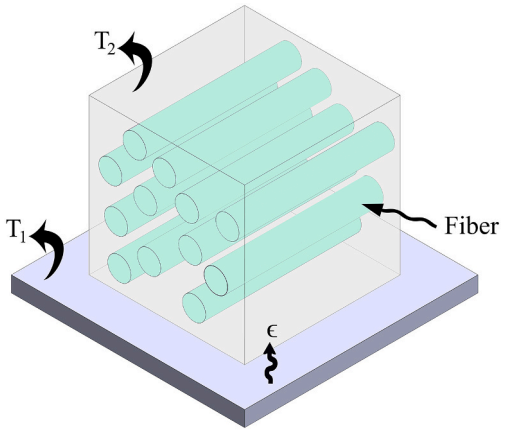

Fig. 5. Schematic representation for calculation of radiative thermal conductivity.

Similar to effective thermal conductivity, the expression used for radiative thermal conductivity needs to be modified. Since this expression is based on radiation between fibers, porosity influences this calculation, and ν_s should be replaced by $\nu_s + \varepsilon_i$.

Therefore, determining whether a region is optically thin or thick and applying an appropriate model is essential. Comparing the magnitude of radiative thermal conductivity to the total heat transfer offers a clear perspective on whether it is negligible. If it is not negligible, this comparison also reveals its magnitude and contribution to the overall thermal performance of fibrous materials.

2.2.4. *Numerical solution for determining fiber thermal conductivity*

After discussing the various modes of heat transfer in fibrous materials and the experimental measurements of sample thermal conductivity, the only remaining unknown parameter in eq. (3) is the thermal conductivity of the fiber itself. Therefore, the following steps must be taken to determine its value:

1. Porosity and volume fraction calculation in nonwoven fabric structures: Calculate the volume fraction of the fiber, inner porosity, outer porosity, and total porosity of the fabric structure using the expressions provided in the previous sections, including eq. (1) and (10) to (12).

2. Initial guess: Make an initial guess for the fiber's thermal conductivity, k_s.
3. Calculate the axial and transverse thermal conductivities of the fiber using eqs. (7) and (8) and determine the thermal conductivity of the fiber composite (including solid fiber and stationary inner air), $k_{s,ave}$, using eq. (9).
4. Effective thermal conductivity calculation: Use eq. (6) along with eqs. (4) and (5), incorporating volume fraction and thermal conductivity adjustments as described in the relevant section.
5. Radiative thermal conductivity calculation: Calculate the radiative thermal conductivity using eq. (14), incorporating adjustments based on the volume fraction described in the relevant section.
6. Convergence: Ensure that the absolute difference between k_{sample} and the sum of k_{eff} and k_{rad} is minimized.
7. Iterative adjustment: If the convergence criterion is not met, iteratively modify the initial guess using the Newton-Raphson method. Given the nonlinear nature of the final expression, repeat the process until the convergence criterion is satisfied.
8. Repetition for similar samples: To improve accuracy, calculate the fiber's thermal conductivity for each fiber type (kapok, MW, and PLA) across different porosities by repeating this process for all samples composed of the same fiber type.
9. Determine the final thermal conductivity, k_s, by averaging the results to obtain a reliable value for each fiber, and recalculate the axial and transverse thermal conductivities using eqs. (7) and (8).

This methodology is implemented using a Fortran code that takes as inputs the mass and volume of the fiber samples, along with the measured thermal conductivity from the Trident device. A detailed flowchart outlining these steps is provided as a supplementary file (Apprendix_1).

Table 2 provides a summary of key parameters for the kapok, MW, and PLA fiber samples, including bulk density, thickness, solid volume fraction, inner porosity, outer porosity, and total porosity.

2.2.5. Thermal conductivity analysis of the nonwoven fabric mixture

In this section, the thermal conductivity of fiber mixtures is investigated, focusing on the combination of different fiber types. This approach allows the unique properties of each fiber to be utilized while ensuring structural stability. Unlike previous studies, where nonwoven fabric mixtures composed of a single fiber type are primarily examined under varying conditions (e.g., different diameters or hollowness) [37,46], mixtures with distinct densities are explored. As a case study, a blend comprising 50 % PLA, 25 % MW, and 25 % kapok fibers is analyzed. A comprehensive summary of three such blend samples, including the corresponding volume fractions (calculated based on fiber densities), and the resulting inner, outer, and total porosities, is presented in Table 3.

To calculate k_{eff} using eq. (4) to (6), an average value for the thermal conductivity of the three fibers is required. This necessitates using the calculated thermal conductivity for each fiber, based on the methodology outlined in Section 2.2.4. The thermal conductivity values for the hollow fibers of kapok and MW are then modified using eq. (7) and (8) . Finally, the average thermal conductivity for the fiber unity is calculated using eq. (15). For each component, x_i is determined based on eq. (16) where v_i represents the volume fraction for each fiber component [46]:

$$k_s = \sum_{i=1}^{n=3} x_i \times k_i \tag{15}$$

$$x_i = \frac{v_i}{\sum_{i=1}^{n=3} v_i} \tag{16}$$

After calculating k_s, which reflects the thermal conductivity of the fiber unity, eq. (4) to (6) can then be used to calculate k_{eff} . Here, similar to the methodology discussed previously for a single fiber type, the modifications to v_s and v_f must also be applied.

Additionally, for calculating the radiative thermal conductivity k_{rad} of the fiber mixture in eq. (2), given that the outer porosity is approximately 97 %, eq. (14) can be utilized. However, as this equation includes a term for the fiber diameter, it is reasonable to use the mean diameter of the fibers in the mixture for this calculation.

All the considerations and expressions outlined in this section are implemented in a Fortran code, where all calculations are explicitly defined. A detailed flowchart outlining these steps is provided as a supplementary file (Apprendix_2).

To verify the results of the thermal conductivity obtained through this theoretical approach, a bench test is developed to compare the experimental measurements with the theoretical predictions. The methodology and operation of this bench test are discussed in the next section.

Table 2
Key parameters of fiber samples, including bulk density, thickness, solid volume fraction, inner porosity, outer porosity, and total porosity.

Fiber type	Sample ID	ρ_{bulk} (kg/m^3)	L (mm)	v_s (%)	ε_i (%)	ε_o (%)	ε (%)
Kapok	K1	7.345	6.00	0.473	3.257	96.270	99.527
	K2	11.018	4.00	0.709	4.886	94.404	99.291
	K3	22.035	2.00	1.418	9.772	88.809	98.581
	K4	39.743	7.00	2.558	17.625	79.816	97.441
	K5	59.928	7.40	3.858	26.577	69.563	96.142
	K6	80.777	5.49	5.200	35.823	58.977	94.750
	K7	120.409	7.00	7.751	53.399	38.850	92.249
	K8	159.935	5.27	10.296	70.928	18.776	89.705
MW	M1	8.013	5.50	0.465	2.710	96.824	99.534
	M2	11.018	4.00	0.640	3.727	95.633	99.360
	M3	22.035	2.00	1.280	7.453	91.266	98.720
	M4	40.923	7.00	2.378	13.842	83.780	97.622
	M5	60.205	7.00	3.498	20.364	76.138	96.502
	M6	79.515	5.30	4.620	26.896	68.484	95.380
	M7	122.420	7.20	7.112	41.408	51.479	92.887
	M8	149.901	5.88	8.710	50.704	40.586	91.290
PLA	P1	22.954	6.00	1.797	–	98.202	98.202
	P2	39.349	7.00	3.081	–	96.919	96.919
	P3	59.417	7.00	4.652	–	95.347	95.347
	P4	78.475	5.30	6.145	–	93.855	93.855
	P5	157.844	5.27	12.360	–	87.640	87.640

Table 3
Properties of nonwoven fabric samples with a 50 % PLA, 25 % MW, and 25 % kapok fiber.

Sample ID	Area Density (gsm)	Area (mm^2)	L (mm)	ρ_{bulk} (kg/m^3)	v_{kapok} (%)	v_{MW} (%)	v_{PLA} (%)	ε_i (%)	ε_o (%)	ε (%)
V1	108.53	106,534.70	10.20	10.640	0.171	0.154	0.208	2.080	97.385	99.466
V2	147.61	98,158.33	15.70	9.402	0.151	0.136	0.184	1.838	97.690	99.528
V3	250.13	99,562.67	22.30	11.216	0.180	0.163	0.219	2.193	97.244	99.437

2.2.6. Bench test measurements for the thermal conductivity of the fiber mixture

The thermal conductivity of the samples is measured using a guarded hot plate apparatus, as shown in Fig. 6. The apparatus consists of three zones: the bottom zone, the measuring (central) zone, and the ring guard zone surrounding the measuring zone. Each zone is independently heated and controlled to maintain a temperature of 35 ± 0.2 °C. The apparatus is placed in a chamber where the ambient temperature is maintained at 20 ± 1 °C and relative humidity of 65 % ± 5, creating a temperature gradient of 15 °C between the top and bottom of the samples. Three tests per sample were conducted.

Once a steady state was achieved, data is collected over a 20-min period (one value per second) and averaged. Each sample was tested under the same conditions, with three repetitions performed for accuracy. Thermal conductivity of the sample is calculated using eq. (17):

$$k_{sample} = \frac{Q \times L}{A \times (T_m - T_a)} \tag{17}$$

where L is the thickness of the fabric structure, Q is the heating power supplied to the measuring zone of the guarded hot plate, A is the area of the measuring zone, and T_m as well as T_a are the temperature of the measuring zone and the ambient temperature, respectively.

This bench test was designed according to the specifications outlined in the ISO 11092 [47], and was validated using three different fabric structures. These structures were previously tested at an independent textile laboratory, following the standard's skin model. The results from the bench test showed a difference of less than 5 % between the experimental measurements and the values obtained from the standard testing, confirming the accuracy and reliability of the proposed method.

3. Results and discussions

3.1. Thermal conductivity of nonwoven fabric structures at varying bulk densities

Kapok, MW, and PLA nonwoven fabrics were evaluated to characterize their thermal properties. It is worth noting that, for example in the PLA samples, the standard deviation for thermal conductivity is approximately 100 times lower than the mean value for each density, resulting in error bars that are not visible. This trend is consistent for both kapok and MW samples. As shown in Fig. 7, the thermal conductivity of the fabric structures increases with bulk density, reflecting the combined effects of conduction and radiation heat transfer within the fibers. This trend is consistent with observations for other natural fibers and becomes particularly notable at densities exceeding 30 kg/m^3, as no measurements are reported for densities below this threshold in [48]. The increase in thermal conductivity with bulk density is attributed to the higher proportion of solid material, which enhances conductive heat transfer, as the thermal conductivity of natural fibers exceeds that of air. Additionally, at similar bulk densities, the thermal conductivity of samples made with kapok and MW fibers is consistently higher than that of PLA. This difference may be attributed to fiber diameter, which plays a critical role in radiative heat transfer within fibrous materials. Specifically, fibers with smaller diameters exhibit greater scattering of radiation, leading to higher extinction coefficients and reduced radiative heat transfer [10]. This mechanism accounts for the comparatively lower thermal conductivity observed in PLA samples.

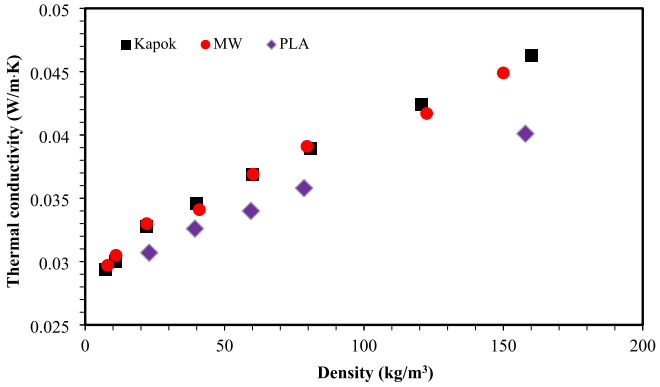

Fig. 7. Thermal conductivity of nonwoven fabrics made of kapok, MW, and PLA at different bulk densities.

3.2. Validation of the method for calculating of the single fiber thermal conductivity

To validate the proposed methodology, data from [36] was utilized. This study reported the thermal conductivity of a solid fiber as 0.130 W/m·K, with experimental measurements of the thermal conductivity of nonwoven fabrics made of this fiber at three different bulk densities. In this validation, the fiber's thermal conductivity was treated as unknown and calculated using the proposed method. The methodology yielded a mean fiber thermal conductivity of 0.129 W/m·K, demonstrating great

(a) (b)

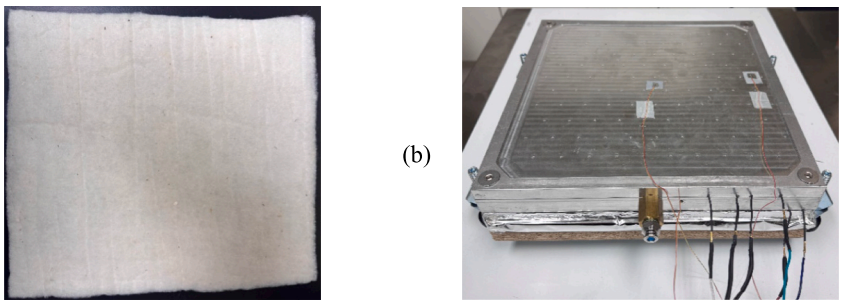

Fig. 6. (a) Nonwoven fabric sample; (b) Guarded hot plate.

agreement with the reported value. This value was obtained by solving three separate equations, each representing one of the three fabric samples analyzed. After obtaining the thermal conductivity results from each of these equations, the average of the three results was calculated to determine the final reported value. Using the calculated fiber conductivity, the thermal conductivity of the nonwoven samples was predicted theoretically and compared to the experimental results, as shown in Fig. 8. The close alignment between experimental and theoretical values, with a maximum difference of 1.8 %, confirms the effectiveness of the methodology. While the analysis of hollow fibers poses greater challenges and no suitable data was found in the literature to apply the approach, this validation using solid fibers underscores the method's potential and adaptability.

3.3. Thermal conductivity of kapok, MW, and PLA

The thermal conductivity of kapok, MW, and PLA fibers was calculated using the proposed method. For kapok and MW, the proposed method was applied to eight samples, resulting in a set of eight nonlinear equations, which were solved and averaged. Similarly, for PLA, the method was applied to five samples, leading to a set of five nonlinear equations whose solutions were averaged. The results, presented in Table 4, include thermal conductivity values for the fibers and anisotropy values for kapok and MW. In contrast, PLA, being a solid fiber, does not exhibit anisotropy. Notably, despite the hollow structure of kapok and MW, their anisotropy is minimal, which may initially seem unexpected. This can be attributed to their thin wall thickness, as reported in Table 1. Based on measurements, the wall thickness is approximately 4 % of the fiber diameter, indicating a highly hollow structure. This characteristic significantly influences the parameter $h = \left(\frac{d_i}{d_o}\right)^2$ in Eqs. (7) and (8), which govern axial and transverse thermal conductivity calculations. As a result, the minimal wall thickness reduces the contrast between these two conductivity components, leading to a less pronounced anisotropic behavior.

Using the mean fiber thermal conductivity values, experimental and theoretical thermal conductivity results of the fabric structures were compared, as shown in Fig. 9 (a) for kapok, (b) for MW, and (c) for PLA. This comparison demonstrates a strong alignment between theoretical predictions and experimental results, with maximum discrepancies of 8.9 %, 10.5 %, and 11.7 % for kapok, MW, and PLA, respectively. These differences can partially be attributed to uncertainties in measurement and calculation tools. While the theoretical model predicts a decrease followed by an increase in thermal conductivity with bulk density, this trend was not observed in the experimental results. To investigate this behavior, it is important to consider the characteristics of fibrous materials, which exhibit an optimal bulk density where thermal conductivity is minimized, as noted in [48]. This optimal point, critical for designing insulation materials, arises from the complex relationship

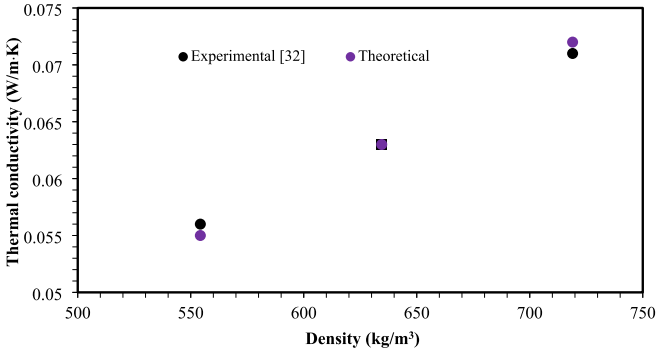

Fig. 8. Comparison of theoretical and experimental thermal conductivity for a fabric structure made of solid fibers.

Table 4
Thermal conductivity and anisotropy of kapok, MW, and PLA fibers.

Fiber type	k_s (W/m·K)	$k_{s,a}$ (W/m·K)	$k_{s,t}$ (W/m·K)	$\frac{k_{s,a}}{k_{s,t}}$
Kapok	0.250	0.054	0.056	0.964
MW	0.307	0.067	0.066	1.015
PLA	0.263	–	–	–

between conduction and radiation. Specifically, at low densities, increased spacing between fibers enhances radiation, while higher densities strengthen conduction and reduce radiation. The ability to calculate the thermal conductivity of a single fiber enables highly accurate predictions of the fabric sample's overall thermal conductivity. This is particularly evident in capturing specific trends observed at very low densities in previous studies [4,10,49] on natural fibers, highlighting the robustness of the proposed method, which is both theoretically predicted by the model and clearly observed in Fig. 9 (a)–(c) for the studied fibers. However, the experimental device, Trident, did not capture this behavior, possibly due to limitations in the measurement system. Even considering this, the overall agreement remains strong, and the observed differences do not impact the validity of the proposed methodology.

3.4. Thermal conductivity of fiber mixtures: comparison between theoretical predictions and experimental bench test results

The thermal conductivity of the three samples (V1, V2, V3), with characteristics outlined in Table 3, was calculated theoretically and compared with the experimental results obtained from the developed bench test, as shown in Fig. 10. Technically, since these samples share the same composition and percentage distribution of materials, they should exhibit similar bulk densities and corresponding thermal conductivity values. However, due to variations that can occur during sample preparation, the experimental results displayed some differences, whereas the theoretical approach yielded thermal conductivity values for the three samples that were very close to each other, presented in Fig. 10. By considering the average of the experimental results, the maximum difference between the theoretical values and this average is 6.6 %, highlighting the accuracy and reliability of the proposed methodology in predicting the thermal conductivity of fabric structures composed of different fibers. Furthermore, an interesting aspect of the theoretical analysis is its ability to differentiate between the contributions of conduction and radiation to heat transfer. Specifically, radiation accounts for 15.1 %, 16.9 %, and 14.9 % of the total heat transfer for samples V1, V2, and V3, respectively, highlighting its significant role in thermal performance and the necessity of accounting for it in the design of effective thermal insulation materials.

3.5. Impact of fiber orientation on thermal conductivity of the nonwoven fabric mixture

In the initial analysis, based on the assumption made in eq. (9), to estimate $k_{s,ave}$, it was considered that half of the fibers are aligned parallel and the other half transverse to the direction of heat transfer. This simplification was necessary because determining the exact proportion of fibers aligned to the direction of heat transfer would require a complex image processing analysis. However, as presented in Fig. 11, analyzing different proportions of fiber orientations—ranging from 10 % to 90 % aligned parallel to the direction of heat transfer—reveals that, when compared to the initial assumption of 50 %, no noticeable change in the thermal conductivity of the sample was observed. This outcome is attributed to the high porosity of the V2 sample, approximately 99.5 %, where changes in fiber orientation have minimal impact on the overall thermal conductivity. Fiber orientation has a more pronounced effect in

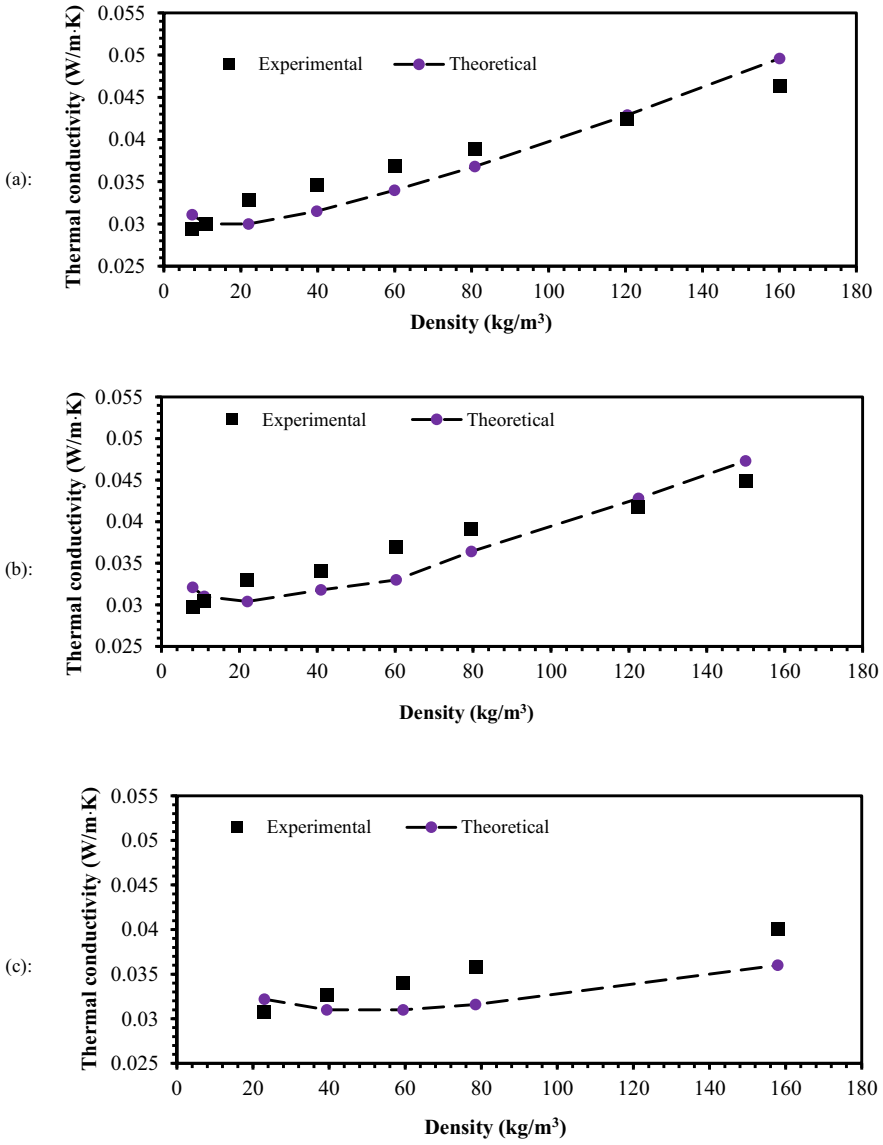

Fig. 9. Comparison of theoretical and experimental thermal conductivity of fabric structures made of (a) kapok, (b) MW, and (c) PLA.

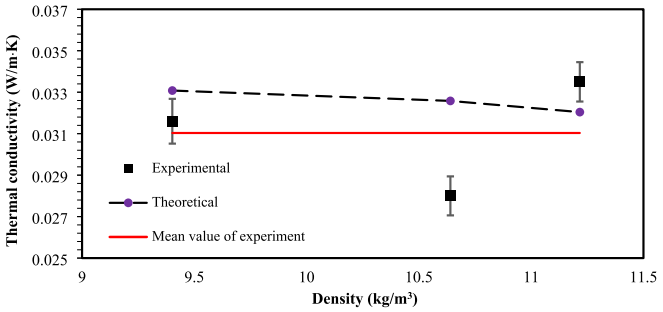

Fig. 10. Comparison of theoretical and experimental thermal conductivity results for samples V1, V2, and V3.

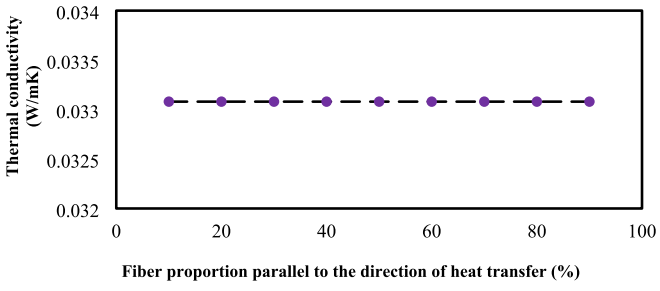

Fig. 11. Thermal conductivity of sample V2 for varying fiber proportion parallel to the direction of heat transfer.

fabric structures composed of solid fibers, which inherently exhibit higher thermal conductivity. In such structures, at lower porosities (e.g., ~65 %), the orientation of individual fibers plays a greater role in determining the overall thermal conductivity of the sample, as presented by Islam and Bhat [36] when investigating the effective thermal conductivity of a sample, incorporating expressions for parallel, perpendicular, and random fiber arrangements. In this study, when k_{eff} is determined using vertical and parallel considerations, distinct results emerge. However, the formulation of k_{eff} in the current study assumes a random fiber arrangement. The assumption made to incorporate $k_{s,ave}$ is necessary for the model and is thoroughly validated in this section to ensure its accuracy.

3.6. Impact of fiber diameter on thermal conductivity of the nonwoven fabric mixture

During the methodology section and in the experimental results of thermal conductivity for samples made from a single type of fiber, it can be concluded that the diameter of the fibers plays a significant role in thermal conductivity, even showing a linear relationship between fiber diameter and radiative thermal conductivity as proposed by eq. (14). Considering the possibility of changing the PLA fiber diameter, the thermal conductivity of sample V2 was analyzed with varying diameters (as reported in Table 1, the diameter of the PLA fiber in the SEM analysis was 15 μm). Fig. 12 illustrates how thermal conductivity changes with different fiber diameters in sample V2. By reducing the PLA fiber diameter to 1 μm, thermal conductivity decreases by approximately 6.3 % compared to the original PLA fiber. When designing insulation materials, lower thermal conductivity is typically desired. Therefore, this reduction in thermal conductivity can be a consideration in the design of thermal insulating materials.

4. Conclusion

This study highlights the importance of understanding the thermal conductivity of natural fibers, particularly hollow fibers, for their application in insulation materials. Using a combined theoretical and experimental approach, the thermal conductivity of individual natural fibers was determined, with a specific focus on hollow fibers such as kapok and MW, alongside solid PLA. The methodology provides valuable insights into the behavior of natural fibers, contributing to advancements in the design of sustainable and efficient thermal insulation materials. Key findings demonstrate that hollow fibers exhibit minimal anisotropy, contrary to initial assumptions. This can be attributed to their thin wall thickness of kapok and MW. Based on measurements, the wall thickness is approximately 4 % of the fiber diameter, indicating a highly hollow structure. The minimal anisotropy observed suggests that the thermal conductivity remains nearly uniform in different directions. The study also explored the thermal conductivity of a nonwoven fabric structure composed of the studied fibers. Theoretical analysis revealed an important distinction between conduction and radiation contributions to heat transfer. Specifically, radiation accounts for approximately 15 % of the total heat transfer in the samples with a porosity of around 99.5 %, highlighting the increasing role of radiative effects in highly porous structures. Further analysis investigated the effects of fiber orientation and diameter. While fiber orientation showed negligible impact in highly porous structures due to the low fiber volume fraction, fiber diameter significantly influenced radiative thermal conductivity. By reducing the PLA fiber diameter from 15 μm to 1 μm, the thermal conductivity of the fabric structure of V2 decreased by approximately 6.3 % compared to the original PLA fiber. This reduction emphasizes the critical role of fiber geometry in optimizing insulation performance. By integrating theoretical and experimental methods, this research provides a robust framework for evaluating the thermal conductivity of fibers and their composites. The findings offer practical guidance for developing sustainable, high-efficiency insulation materials, addressing the challenges of accurately characterizing and optimizing the thermal behavior of natural fibers.

CRediT authorship contribution statement

Seyyed Mohsen Mortazavinejad: Software, Data curation, Investigation, Writing – original draft, Methodology. **Mostafa Alakhdar:** Writing – original draft, Data curation, Investigation. **Ludwig Vinches:** Writing – review & editing, Project administration, Supervision, Investigation. **Stéphane Hallé:** Writing – review & editing, Investigation, Supervision, Conceptualization.

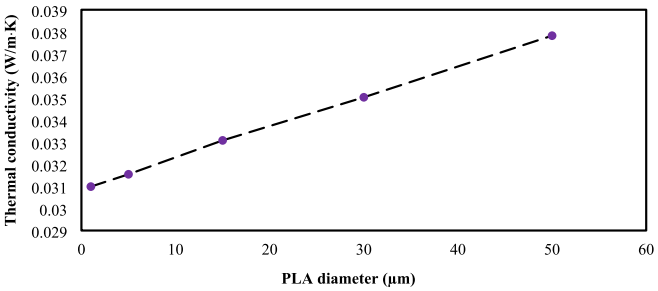

Fig. 12. Thermal conductivity of sample V2 for varying PLA fiber diameters.

Declaration of generative AI and AI-assisted technologies in the writing process

During the preparation of this work, the authors used ChatGPT-4 in order to improve readability and language. After using this tool, the authors reviewed and edited the content as needed and take full responsibility for the content of the publication.

Declaration of competing interest

The authors declare that they have no known competing financial interests or personal relationships that could have appeared to influence the work reported in this paper.

Acknowledgements

This work was supported by a financial support of our industrial partners, Logistik Unicorp Inc. and Eko-Terre, as well as a grant from PRIMA Québec (N° R23-13-001) and the Natural Sciences and Engineering Research Council of Canada (ALLRP 566738 - 21). The authors would like to thank Dr. Marwa Sta for her assistance.

Appendix A. Supplementary data

Supplementary data to this article can be found online at https://doi.org/10.1016/j.icheatmasstransfer.2025.109269.

Data availability

Data will be made available on request.

References

[1] A. Patnaik, M. Mvubu, S. Muniyasamy, A. Botha, R.D. Anandjiwala, Thermal and sound insulation materials from waste wool and recycled polyester fibers and their biodegradation studies, Energ. Build. 92 (Apr. 2015) 161–169, https://doi.org/10.1016/j.enbuild.2015.01.056.
[2] A.M. Papadopoulos, State of the art in thermal insulation materials and aims for future developments, Energ. Build. 37 (1) (2005), https://doi.org/10.1016/j.enbuild.2004.05.006.
[3] W. Villasmil, L.J. Fischer, J. Worlitschek, A Review and Evaluation of Thermal Insulation Materials and Methods for Thermal Energy Storage Systems, 2019, https://doi.org/10.1016/j.rser.2018.12.040.
[4] K. Manohar, A. Adeyanju, A comparison of banana fiber thermal insulation with conventional building thermal insulation, Br. J. Appl. Sci. Technol. 17 (3) (2016), https://doi.org/10.9734/bjast/2016/29070.
[5] L.F. Liu, et al., The Development History and Prospects of Biomass-Based Insulation Materials for Buildings, 2017, https://doi.org/10.1016/j.rser.2016.11.140.
[6] M.R. Ponnada, K. P, Construction and demolition waste management – a review, Int. J. Adv. Sci. Technol. 84 (2015), https://doi.org/10.14257/ijast.2015.84.03.
[7] C.S. Boland, R. De Kleine, G.A. Keoleian, E.C. Lee, H.C. Kim, T.J. Wallington, Life cycle impacts of natural fiber composites for automotive applications: effects of renewable energy content and lightweighting, J. Ind. Ecol. 20 (1) (2016), https://doi.org/10.1111/jiec.12286.
[8] D. Illera, J. Mesa, H. Gomez, H. Maury, Cellulose Aerogels for Thermal Insulation in Buildings: Trends and Challenges, 2018, https://doi.org/10.3390/coatings8100345.

[9] M. Alakhdar, L. Vinches, S. Hallé, Assessing thermal resistance of a nonwoven textile under wind exposure: challenging ISO 9920 with experimental insights, J. Ind. Text. 55 (Mar. 2025), https://doi.org/10.1177/15280837251328908.
[10] X. Lian, L. Tian, Z. Li, X. Zhao, Thermal conductivity analysis of natural fiber-derived porous thermal insulation materials, Int. J. Heat Mass Transf. 220 (2024), https://doi.org/10.1016/j.ijheatmasstransfer.2023.124941.
[11] D. Csanády, O. Fenyvesi, B. Nagy, Heat transfer in straw-based thermal insulating materials, Materials 14 (16) (2021), https://doi.org/10.3390/ma14164408.
[12] R. El-Sawalhi, J. Lux, P. Salagnac, Estimation of the thermal conductivity of hemp based insulation material from 3D tomographic images, Heat Mass Transf. Waerme- und Stoffuebertragung 52 (8) (2016), https://doi.org/10.1007/s00231-015-1674-4.
[13] R. Stapulionienė, S. Vaitkus, S. Vėjelis, A. Sankauskaitė, Investigation of thermal conductivity of natural fibres processed by different mechanical methods, Int. J. Precis. Eng. Manuf. 17 (10) (2016), https://doi.org/10.1007/s12541-016-0163-0.
[14] L.D. Hung Anh, Z. Pásztory, An overview of factors influencing thermal conductivity of building insulation materials, Elsevier Ltd. (Dec. 01, 2021), https://doi.org/10.1016/j.jobe.2021.102604.
[15] Shabaridharan, A. Das, Study on heat and moisture vapour transmission characteristics through multilayered fabric ensembles, Fibers Polym. 13 (4) (2012), https://doi.org/10.1007/s12221-012-0522-0.
[16] U. Hammerschmidt, J. Hameury, R. Strnad, E. Turzó-Andras, J. Wu, Critical review of industrial techniques for thermal-conductivity measurements of thermal insulation materials, Int. J. Thermophys. 36 (7) (2015), https://doi.org/10.1007/s10765-015-1863-x.
[17] G. Xu, J.M. Lamanna, J.T. Clement, M.M. Mench, Direct measurement of through-plane thermal conductivity of partially saturated fuel cell diffusion media, J. Power Sources 256 (2014), https://doi.org/10.1016/j.jpowsour.2014.01.015.
[18] J.K. Carson, S.J. Lovatt, D.J. Tanner, A.C. Cleland, Thermal conductivity bounds for isotropic, porous materials, Int. J. Heat Mass Transf. 48 (11) (2005), https://doi.org/10.1016/j.ijheatmasstransfer.2004.12.032.
[19] R.L. Hamilton, Thermal conductivity of heterogeneous two-component systems, Ind. Eng. Chem. Fundam. 1 (3) (1962), https://doi.org/10.1021/i160003a005.
[20] L. Gong, Y. Wang, X. Cheng, R. Zhang, H. Zhang, A novel effective medium theory for modelling the thermal conductivity of porous materials, Int. J. Heat Mass Transf. 68 (2014), https://doi.org/10.1016/j.ijheatmasstransfer.2013.09.043.
[21] S. Kawabata, Measurement of Anisotropic Thermal Conductivity of Single Fibre, 1986, https://doi.org/10.4188/transjtmsj.39.12_t184.
[22] V. Asangwing, Optimisation of Formulations of Stabilised Earth Blocks Using Local Natural Fibers for Home Construction, Ph.D. Thesis, ENSET, Douala, 2010.
[23] J.C. Damfeu, P. Meukam, Y. Jannot, Modeling and measuring of the thermal properties of insulating vegetable fibers by the asymmetrical hot plate method and the radial flux method: kapok, coconut, groundnut shell fiber and rattan, Thermochim. Acta 630 (2016), https://doi.org/10.1016/j.tca.2016.02.007.
[24] F.A. Al-Sulaiman, E.M.A. Mokheimer, Y.N. Al-Nassar, Prediction of the thermal conductivity of the constituents of fiber reinforced composite laminates, Heat Mass Transf. Waerme- und Stoffuebertragung 42 (5) (2006), https://doi.org/10.1007/s00231-005-0636-7.
[25] F.A. Al-Sulaiman, Y.N. Al-Nassar, E.M.A. Mokheimer, Numerical prediction of the thermal conductivity of fibers, Heat Mass Transf. Waerme- und Stoffuebertragung 42 (5) (2006), https://doi.org/10.1007/s00231-005-0058-6.
[26] S. Sanchez-Diaz, C. Ouellet, S. Elkoun, M. Robert, Evaluating the properties of native and modified milkweed floss for applications as a reinforcing fiber, J. Nat. Fibers 20 (1) (2023), https://doi.org/10.1080/15440478.2023.2174630.
[27] R.H. Sangalang, Kapok fiber- structure, characteristics and applications: a review, Orient. J. Chem. 37 (3) (2021), https://doi.org/10.13005/ojc/370301.
[28] M.S. Barkhad, B. Abu-Jdayil, M.Z. Iqbal, A.H.I. Mourad, Thermal insulation using biodegradable poly(lactic acid)/date pit composites, Constr. Build. Mater. 261 (2020), https://doi.org/10.1016/j.conbuildmat.2020.120533.
[29] T. Dong, F. Wang, G. Xu, Theoretical and experimental study on the oil sorption behavior of kapok assemblies, Ind. Crop. Prod. 61 (2014) 325–330, https://doi.org/10.1016/j.indcrop.2014.07.020.
[30] S. Meiwu, X. Hong, Yu Weidong, The fine structure of the kapok fiber, Text. Res. J. 80 (2) (2010), https://doi.org/10.1177/0040517508095594.
[31] M.S. Barkhad, B. Abu-Jdayil, A.H.I. Mourad, M.Z. Iqbal, Thermal insulation and mechanical properties of polylactic acid (PLA) at different processing conditions, Polymers (Basel) 12 (9) (2020), https://doi.org/10.3390/POLYM12092091.
[32] M.L. Voumbo, A. Wereme, S. Gaye, M. Adj, G. Sissoko, Characterization of the thermophysical properties of kapok, Res. J. Appl. Sci. Eng. Technol. 2 (2) (2010).
[33] S. Sanchez-Diaz, S. Elkoun, M. Robert, Thermal insulation properties of milkweed floss nonwovens: influence of temperature, relative humidity, and fiber content, J. Compos. Sci. 8 (1) (2024), https://doi.org/10.3390/jcs8010016.
[34] D.A. Nield, A. Bejan, Convection in porous media, 2013, https://doi.org/10.1007/978-1-4614-5541-7.
[35] R. Arambakam, H.V. Tafreshi, B. Pourdeyhimi, Modeling performance of multi-component fibrous insulations against conductive and radiative heat transfer, Int. J. Heat Mass Transf. 71 (2014), https://doi.org/10.1016/j.ijheatmasstransfer.2013.12.031.
[36] S. Islam, G. Bhat, A model for predicting thermal conductivity of porous composite materials, Heat Mass Transf. Waerme- und Stoffuebertragung 59 (11) (2023), https://doi.org/10.1007/s00231-023-03380-w.
[37] V. Dupade, R. Kumari, B. Premachandran, R.S. Rengasamy, P. Talukdar, Effect of layering sequence and ambient temperature on thermal insulation of multilayer high bulk nonwoven under extreme cold temperatures, J. Ind. Text. 51, no. 2_suppl (2022), https://doi.org/10.1177/15280837221097284.
[38] R.B. Bird, W.E. Stewart, E.N. Lightfoot, Transport Phenomena, Revised 2nd edition, 2006 [Online]. Available: https://www.amazon.com/Transport-Phenomena-Revised-Byron-Bird/dp/0470115394.
[39] T. Dong, F. Wang, G. Xu, Theoretical and experimental study on the oil sorption behavior of kapok assemblies, Ind. Crop. Prod. 61 (2014), https://doi.org/10.1016/j.indcrop.2014.07.020.
[40] H. Shen, Y. Xu, F. Wang, J. Wang, L. Tu, Numerical analysis of heat and flow transfer in porous textiles - influence of wind velocity and air permeability, Int. J. Therm. Sci. 155 (Sep. 2020), https://doi.org/10.1016/j.ijthermalsci.2020.106432.
[41] Y.L. He, T. Xie, Advances of Thermal Conductivity Models of Nanoscale Silica Aerogel Insulation Material, 2015, https://doi.org/10.1016/j.applthermaleng.2015.02.013.
[42] M.F. Modest, Radiative Heat Transfer, 2nd edition, 2003, https://doi.org/10.1016/B978-0-12-503163-9.X5000-0.
[43] C. Bankvall, Heat transfer in fibrous materials, J. Test. Eval. 1 (3) (1973) 235–243, https://doi.org/10.1520/jte10010j.
[44] S. Yuan Zhao, B. Ming Zhang, X. Dong He, Temperature and pressure dependent effective thermal conductivity of fibrous insulation, Int. J. Therm. Sci. 48 (2) (2009), https://doi.org/10.1016/j.ijthermalsci.2008.05.003.
[45] B. Farnworth, Mechanisms of heat flow through clothing insulation, Text. Res. J. 53 (12) (1983) 717–725, https://doi.org/10.1177/004051758305301201.
[46] T. Yang, et al., Theoretical and experimental studies on thermal properties of polyester nonwoven fibrous material, Materials 13 (12) (2020), https://doi.org/10.3390/ma13122882.
[47] International Organization for Standardization, ISO 11092:2014 - Textiles – Physiological Effects – Measurement of Thermal and Water-Vapour Resistance under Steady-State Conditions (Sweating Guarded-Hotplate Test), Second ed., 2014 no. December.
[48] C. Piégay, P. Glé, E. Gourdon, E. Gourlay, A cylindrical self-consistent modelling of vegetal wools thermal conductivity, Constr. Build. Mater. 232 (2020), https://doi.org/10.1016/j.conbuildmat.2019.117123.
[49] C. Piégay, P. Glé, E. Gourlay, E. Gourdon, S. Marceau, Micro-macro modelling approach of vegetal wools thermal conductivity, Bio-Based Build. Mater. (2022), https://doi.org/10.4028/www.scientific.net/cta.1.421.